Differences Between the Narrow-Angle and Wide-Angle Propagators in the Split-Step Fourier Solution of the Parabolic Wave Equation

James R. Kuttler

***Abstract*— For tropospheric electromagnetic propagation, Maxwell's equations can be reduced to a parabolic wave equation, which is solved by marching over range steps. In each step, the solution is split into a product of three operators. The first and third account for atmospheric and surface variation, while the center operator propagates the field as though in vacuum. This center operator is the object of interest here. Older versions of the method used the narrow-angle propagator, while some recent versions use the wide-angle propagator. It was thought that the wide-angle propagator was entirely superior to the narrow-angle propagator, but some artifacts observed in recent experiments have led to the present investigation. The two propagators are examined numerically and analytically and found to exhibit subtle differences at large angles from the horizontal. This has required modifications to the way in which sources are created for starting the split-step solution. The narrow- and wide-angle propagators are also compared on two problems with analytic solutions to quantify the improvement of the wide-angle over the narrow-angle**

***Index Terms*— Parabolic wave equation, propagators, tropospheric propagation.**

I. Introduction

THE parabolic approximation/Fourier split-step algorithm [1], [2] is a powerful method for modeling electromagnetic propagation through inhomogeneous atmosphere and above the surface of the earth, which may have large- and small-scale roughness plus various dielectric properties. Assuming azimuthal symmetry, Maxwell's equations can be reduced to a two-dimensional scalar Helmholtz equation, which is then factored into forward and backward propagating pieces. Only the forward propagating part is used. This is a parabolic wave equation that is solved by marching over range steps. In each step the solution operator is split into a product of three operators: the first and third account for atmospheric and surface variation, while the center operator propagates the field as though in vacuum and is the object of interest here.

Older versions of the method used the narrow-angle propagator. It performs admirably for problems where the field propagates along paths nearly horizontal to the surface. It is good for propagation at angles up to about 10° from the local horizontal. Some of the more recent versions of the method use a wide-angle propagator. A wide-angle capability is needed for propagation over terrain with prescribed features such as mountains and valleys, which are large compared to the wavelength and cause reflection and diffraction of the field into large angles.

It has been presumed that the wide-angle propagator was, in all respects, superior to the narrow-angle propagator in that it is expected to give the same answer in problems where the narrow-angle is known to work well and to continue to give accurate answers for problems with angles of propagation as large as 25° or more. However, in some recent experiments with problems over terrain with specified obstacles such as steps, ramps, and pyramids [3], [4], some subtleties appeared in the implementation and interpretation of the narrow-angle and wide-angle propagators that affect the way sources are defined for use with the wide-angle propagator. This is the subject of this note.

As indicated above, the propagator is separated from the atmospheric and surface effects by the splitting of the operator, so it suffices to consider the pure free-space problem with no boundaries present. Then the wide-angle and narrow-angle propagators and the true solution to the propagation problem can be examined analytically. It turns out that the wide-angle propagator is indeed superior to the narrow-angle propagator and that the differing behavior in the two propagators only shows up at large angles from horizontal. However, these differences will be of importance for problems with propagation at large angles.

In this paper, derivations of the narrow- and wide-angle propagators are briefly reviewed in the context of solutions to the Helmholtz equation and both propagators are then evaluated numerically for the free-space problem. Then, referring to basic antenna theory, the two solutions are compared with "truth" as derived for a finite line source. This comparison between the antenna solution and the narrow- and wide-angle parabolic wave equation solutions will lead to a proper interpretation of observed numerical results and will also indicate how wide-angle sources should be generated for electromagnetic propagation problems.

Finally, two examples which have analytic solutions, the knife-edge and the sinusoidal surface, will be solved using the two propagators, so that improvements of the wide-angle propagator over the narrow-angle propagator can be seen and quantified.

Manuscript received October 26, 1998; revised May 20, 1999.

The author is with the Applied Physics Laboratory, The Johns Hopkins University Laurel, MD 20723 USA.

Publisher Item Identifier S 0018-926X(99)07074-X.

II. Derivation of the Narrow-Angle and Wide-Angle Propagators

In free-space with no boundaries, if Maxwell's equations are expressed in spherical coordinates and all sources are on the z axis, then all components of the fields are independent of the azimuth angle. This symmetry assumption simplifies the Maxwell equations, which can then be decomposed into two cases—vertical and horizontal polarization. These independent cases can each be reduced to a two-dimensional scalar equation in H_ϕ or E_ϕ, which, in turn, can be manipulated into a Helmholtz equation (see [1])

$$\frac{\partial^2 U}{\partial x^2} + \frac{\partial^2 U}{\partial z^2} + k^2 n^2 U = 0 \tag{1}$$

where $U = \sqrt{x} H_\phi$ or $\sqrt{x} E_\phi$, respectively, for vertical or horizontal polarization. In the general case, the term n^2 is a variable depending on the index of refraction of the atmosphere and the surface roughness, but for free-space without boundaries $n^2 = 1$. Equation (1) is factored into

$$\left[\frac{\partial}{\partial x} + i\sqrt{k^2 + \frac{\partial^2}{\partial z^2}}\right]\left[\frac{\partial}{\partial x} - i\sqrt{k^2 + \frac{\partial^2}{\partial z^2}}\right] U = 0$$

and only one piece is solved

$$\frac{\partial U}{\partial x} = i\sqrt{k^2 + \frac{\partial^2}{\partial z^2}}\, U \tag{2}$$

giving the propagation in the forward or positive x direction.

Equation (2) is the wide-angle parabolic wave equation [5], [6] and its solution is

$$U(x,z) = \exp\left[ix\sqrt{k^2 + \frac{\partial^2}{\partial z^2}}\right] U(0,z) \tag{3}$$

where $U(0,z)$ is the given source function on the z axis and where the exponential of a square root of an operator can be interpreted as a power series in the operator. Next, (3) is Fourier transformed. Since there are no boundaries, the full exponential Fourier transform is used. Recall that the Fourier transform of a derivative is ip times the transform, where p is the transform variable. Since the exponential in (3) is a power series in $\partial^2/\partial z^2$, applying the Fourier transform results in the same power series in $-p^2$, so (3) becomes

$$\mathcal{F}U(x,p) = \exp[ix\sqrt{k^2 - p^2}]\mathcal{F}U(0,p). \tag{4}$$

The solution is obtained by inverse transforming

$$U(x,z) = \int_{-\infty}^{\infty} U(0,s)\frac{1}{2\pi}\int_{-\infty}^{\infty} e^{i(z-s)p} e^{ix\sqrt{k^2-p^2}}\, dp\, ds.$$

Thus, the solution to the wide-angle parabolic equation (2) is given by the convolution of the fundamental solution

$$W(x,z) \equiv \frac{1}{2\pi}\int_{-\infty}^{\infty} e^{izp} e^{ix\sqrt{k^2-p^2}}\, dp \tag{5}$$

with the source term $U(0,s)$.

The narrow-angle parabolic equation can be obtained from (2) by taking only the first two terms of the series expansion of the square-root operator

$$\sqrt{k^2 + \frac{\partial^2}{\partial z^2}} \approx k + \frac{1}{2k}\frac{\partial^2}{\partial z^2}$$

resulting in

$$\frac{\partial U}{\partial x} = i\left(k + \frac{1}{2k}\frac{\partial^2}{\partial z^2}\right) U. \tag{6}$$

Again using Fourier transforms, the solution to the narrow-angle parabolic equation (6) is given by the convolution of the fundamental solution

$$N(x,z) \equiv \frac{e^{ikx}}{2\pi}\int_{-\infty}^{\infty} e^{izp} e^{-ixp^2/2k}\, dp \tag{7}$$

with the source term $U(0,s)$.

III. Evaluation of the Wide-Angle and Narrow-Angle Propagators

The fundamental solutions $W(x,z)$ and $N(x,z)$ can be evaluated numerically using FFT's. For k corresponding to a frequency of 1 GHz, a range x of 150 ft and a transform size of 2^{10}, $|N(x,z)|^2$ is plotted in Fig. 1(a) in decibels after normalizing by multiplying by $2\pi x/k$. This normalization makes the field magnitude unity (0 dB) at beam center, as can be seen in the figure. The normalization factor will be analytically justified in the following. Since the far-field pattern of an antenna is the Fourier transform of the antenna aperture distribution and the fundamental solution essentially propagates a point source, this result looks correct. However, similarly plotting $|W(x,z)|^2$ with the same frequency, range, transform size, and the same normalization factor produces the result shown in Fig. 1(b). This figure looks a little strange and is essentially what prompted the investigation reported here.

Both the narrow-angle and wide-angle propagators can also be expressed analytically. In (7) complete the square in the exponent and change variables making it a well-known Fresnel integral [7, sec. VII-C]. So the narrow-angle propagator is

$$\sqrt{\frac{k}{2\pi i x}} e^{ik(x+z^2/2x)}. \tag{8}$$

This could also have been found by solving the constant coefficient parabolic equation (6) using the methods of [8, ch. II]. The normalization factor and the plot in Fig. 1(a) are verified.

The wide-angle propagator in (5) can be evaluated from differentiating a formula found in [9, p. 823] or in [10, p. 199]. Or it can be gotten from inverting and differentiating formulas (35) and (41) in [11, pp. 55–56]. In any event

$$W(x,z) = \frac{ikxH_1^{(1)}(kr)}{2r}, \quad r = \sqrt{x^2 + z^2}. \tag{9}$$

Using the asymptotic value for the Hankel function $H_1^{(1)}$ from [7, 9.2.3]

$$W(x,z) \sim \sqrt{\frac{k}{2\pi i}}\,\frac{xe^{ikr}}{r^{3/2}}. \tag{10}$$

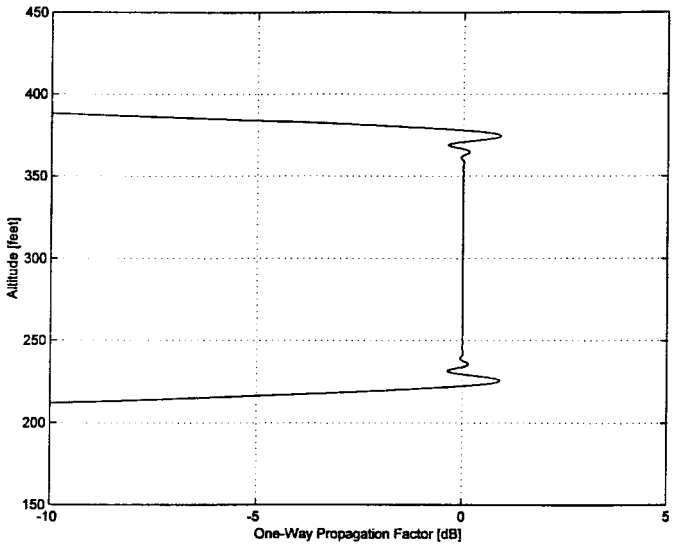

(a)

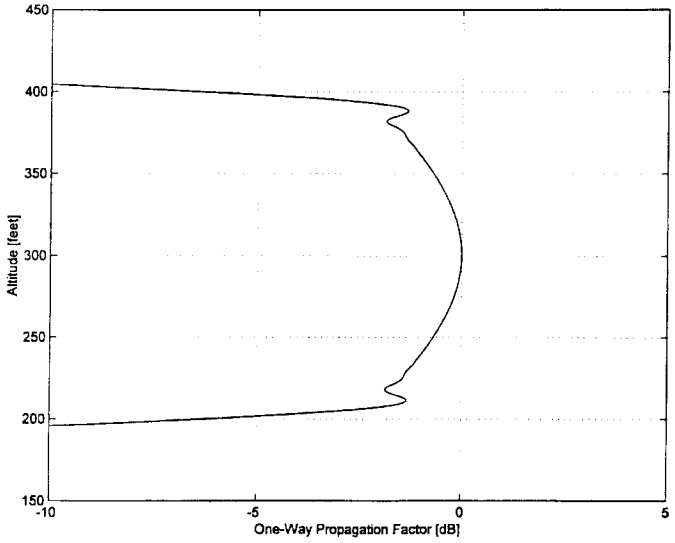

(b)

Fig. 1. 1-GHz propagation of a point source to 150 ft by (a) narrow-angle and (b) wide-angle.

Thus, $|W(x,z)|^2$, after multiplying by the same normalizing factor $2\pi x/k$, is $\cos^3\theta$, where $\theta = \tan^{-1}(z/x)$ and this agrees with Fig. 1(b).

IV. What Is Truth?

The following discussion is an abbreviated version of material, which can be found in, e.g., [12, chs. 3, 4] and elsewhere. If the source $\boldsymbol{J} = a(z)\boldsymbol{u}_z$ is a current distribution on the z axis, oriented in the z direction and concentrated in the interval $-L/2 \le z \le L/2$, then a vector potential for Maxwell's equations is

$$\boldsymbol{A}(x,z) = \boldsymbol{u}_z \frac{\mu}{4\pi} \int_{-L/2}^{L/2} \frac{e^{ik\sqrt{x^2+(z-z')^2}}}{\sqrt{x^2+(z-z')^2}} a(z')\, dz'.$$

In the far field, make the estimate

$$\sqrt{x^2+(z-z')^2} \approx r - \frac{z}{r}z' + \text{higher terms}.$$

(So the far field is defined by $r \gg L/2$.) In the denominator, retain only the first term r, but in the exponential use the first two terms. Thus

$$\boldsymbol{A} \approx \boldsymbol{u}_z \frac{\mu e^{ikr}}{4\pi r} \int_{-L/2}^{L/2} e^{-ikz'z/r} a(z')\, dz'.$$

The integral is the Fourier transform $F(k\sin\theta)$ of the current distribution on the z axis, evaluated at $kz/r = k\sin\theta$. In the far field, $H_r = H_\theta = 0$ and

$$H_\phi = \text{const}\ \frac{xe^{ikr}}{r^2} F(k\sin\theta). \tag{11}$$

This is a derivation of the abovementioned result that the far-field antenna pattern looks like the Fourier transform of the aperture distribution. But the Fourier transform is not the whole story.

In [12, p. 119], $F(k\sin\theta)$ is called the *space factor* and the remaining terms on the right side of (11) are called the *element factor*. The magnitude of the element factor is

$$\frac{x}{r^2} = \frac{\cos^2\theta}{x}. \tag{12}$$

Presumably, (11) is truth. This is the far field which nature, in the form of Maxwell's equations, produces in free-space. Doing a similar analysis after convolving the source with the far-field asymptotic expression for $W(x,z)$ from (10) gives

$$H_\phi = \text{const}\ \frac{e^{ikr}\cos^{3/2}\theta}{x} F(k\sin\theta) \tag{13}$$

so the magnitude of the element factor for the wide-angle propagator is $\cos^{3/2}\theta/x$.

When the exact expression (8) for the narrow-angle propagator is convolved with the source

$$\sqrt{\frac{k}{2\pi ix}} e^{ik(x+z^2/2x)} \int_{-\infty}^{\infty} \exp ik\left(-\frac{zs}{x} + \frac{s^2}{2x}\right) U(0,s)\, ds \tag{14}$$

is obtained. Now, if the aperture distribution is bounded in, say, $-L/2 \le z \le L/2$, then as $x \to \infty$, the term in the exponential $s^2/2x \to 0$ and (14) becomes

$$\sqrt{\frac{k}{2\pi ix}} e^{ik(x+z^2/2x)} F(k\tan\theta).$$

Also

$$x + \frac{z^2}{2x} \approx x\sqrt{1+\frac{z^2}{x^2}} = r.$$

So in the far field of the narrow-angle propagator

$$H_\phi = \text{const}\ \frac{e^{ikr}}{x} F(k\tan\theta). \tag{15}$$

Hence, the magnitude of the element factor for the narrow-angle propagator is $1/x$ and note that its space-factor is $F(k\tan\theta)$.

Near horizontal $r \approx x, \cos\theta \approx 1, \tan\theta \approx \sin\theta$ and (11), (13), and (15) are approximately the same. Away from horizontal they are all different. There, neither the wide-angle propagator nor the narrow-angle propagator exactly

corresponds to truth, but the wide-angle is closer. Moreover, the space factor of the wide-angle propagator agrees with the true space factor, while that of the narrow-angle does not. So it appears that the wide-angle propagator is indeed superior to the narrow-angle propagator. The element factor in the wide-angle propagator has simply not been accounted for correctly.

V. How Should the Wide-Angle Propagator Be Adjusted?

In [13, p. 35] the propagation factor is defined as

$$\frac{|H|}{|H_0|} \tag{16}$$

where H is a field component and H_0 would be its value in free-space. The free-space values of $|H_\phi|$ have been calculated above under various assumptions. Near the horizontal, all these values reduce to $1/x$, so the multiplier that has traditionally been used to obtain the propagation factor is correct for near-horizontal propagation.

Off axis, under the assumption that the fields are generated by a bounded source along the z axis, the magnitude of the true far field will be x/r^2, where r is calculated from an appropriate center in such a source. However, the proper interpretation of (16) should probably be that the propagation factor is the ratio of the magnitude of the field component computed by a particular method (whether nature, narrow-angle, wide-angle, or something else), to the magnitude of its free-space value, *computed by the same method.*

Thus, when computing with the narrow-angle propagator, the multiplier on H_ϕ to get the propagation factor should indeed be x, as has generally been used. However, when using the wide-angle propagator, the appropriate multiplier would be

$$\frac{r^{3/2}}{x^{1/2}} = \frac{x}{\cos^{3/2}\theta}. \tag{17}$$

Fig. 2(a) shows the wide-angle propagator for a 1-GHz point source at range $x = 150$ ft, when multiplied by (17). (Compare with Fig. 1.)

While this is a fine result for a point source in free-space, this is not what should be done in general. The r in (17) is actually path length, which, in an inhomogeneous atmosphere or after reflections from surfaces, is not a readily available quantity. What needs to be done is to adjust the source so that the angle-dependent terms $\cos^{3/2}\theta F(k\sin\theta)$ produce a desired free-space pattern, say $P(\theta)$. So set

$$F(k\sin\theta) = \frac{P(\theta)}{\cos^{3/2}\theta}$$

or

$$F(p) = \frac{k^{3/2}P(\sin^{-1}(p/k))}{(k^2-p^2)^{3/4}} \tag{18}$$

and invert the Fourier transform to determine the source distribution, which, when propagated by the wide-angle, will produce the desired free-space pattern.

This procedure can be illustrated by trying to produce the boxcar or sector pattern of Fig. 2(a) in this way. At first glance, this problem would seem to be trying to put a gain on a point source. The desired pattern is

$$P(\theta) = \begin{cases} 1, & |\theta| < \pi/2, \\ 0, & \text{otherwise} \end{cases}$$

so

$$F(p) = \begin{cases} k^{3/2}(k^2-p^2)^{-3/4}, & |p| < k, \\ 0, & \text{otherwise} \end{cases}$$

which is smoothed with a bandpass filter and produces the source function shown in Fig. 3, the "point source with a gain." When propagated with the wide-angle at 1 GHz to range $x = 150$ ft, the pattern shown in Fig. 2(b) is obtained.

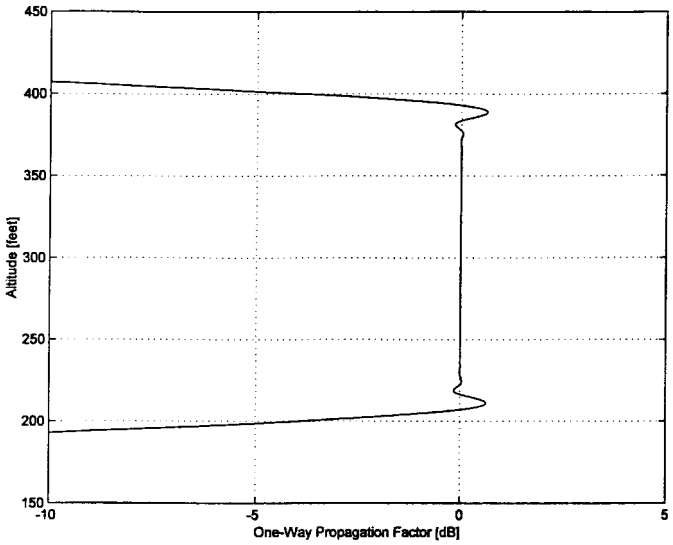

(a)

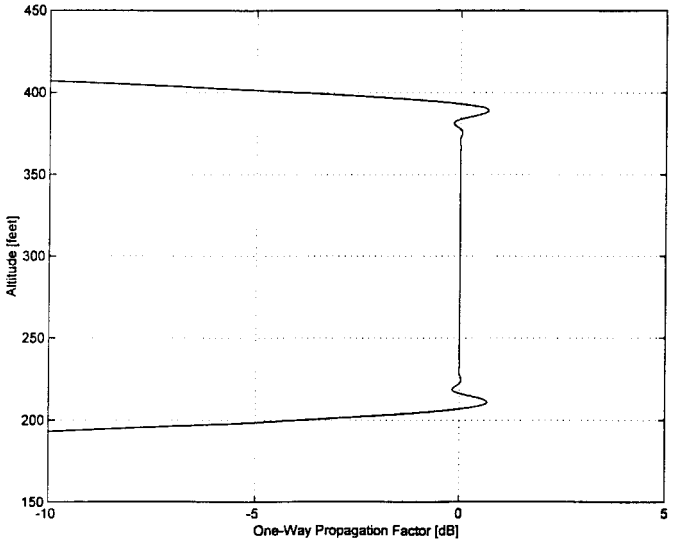

(b)

Fig. 2. 1-Ghz wide-angle propagation to 150 ft of (a) a point source after dividing by $cos^{3/2}\theta$ and (b) a point source with a gain. They are virtually identical.

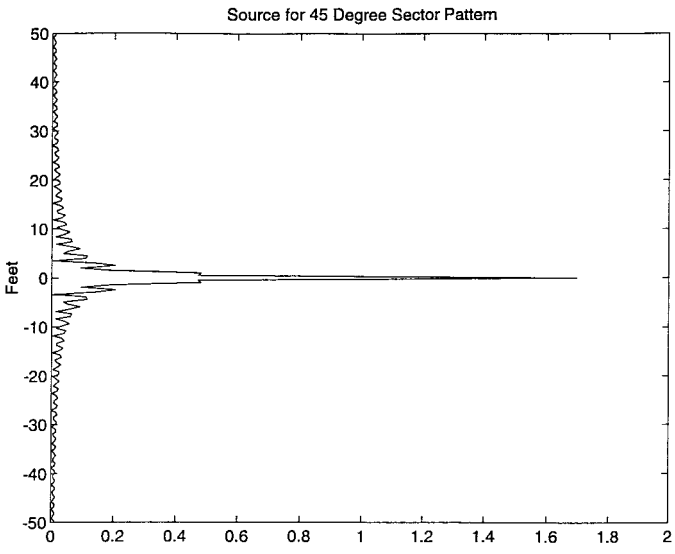

Fig. 3. The "point source with a gain."

VI. Plane Wave Propagation by the Wide-Angle and Narrow-Angle Propagators

Write the wide-angle propagator (5) in a different form. Since it is essentially

$$W(x,z) \approx \frac{1}{2\pi} \int_{-k}^{k} e^{izp} e^{ix\sqrt{k^2-p^2}}\, dp$$

after making the change of variable $p = k\sin\theta$, it becomes

$$\frac{k}{2\pi} \int_{-\pi/2}^{\pi/2} e^{ik(x\cos\theta + z\sin\theta)} \cos\theta \, d\theta. \tag{19}$$

This looks like a plane wave at angle θ with the horizontal, integrated against $\cos\theta$ (which is maximum in the $\theta = 0$ or x direction) over all forward angles $-\pi/2 < \theta < \pi/2$.

This suggests investigating how $W(x,z)$ propagates a plane wave. Suppose then that at $x = 0$ the plane wave source is

$$e^{ikz\sin\gamma} \tag{20}$$

where γ is the angle the direction of propagation makes with the x axis. Now convolve with expression (19) for W. After some manipulations involving interchanging the order of integration and recognizing a formula for the delta distribution, one obtains

$$e^{ik(x\cos\gamma + z\sin\gamma)}$$

for $-\pi/2 < \gamma < \pi/2$ and the wide-angle propagator propagates a plane wave at range zero and angle γ into a plane wave at range x and angle γ.

Next, convolve the plane wave source in (20) with the narrow-angle propagator in (8) to get

$$\exp ik[x(1 - \tfrac{1}{2}\sin^2\gamma) + z\sin\gamma].$$

Now

$$\cos\gamma = 1 - \tfrac{1}{2}\gamma^2 + \tfrac{1}{24}\gamma^4 - \cdots$$

while

$$1 - \tfrac{1}{2}\sin^2\gamma = 1 - \tfrac{1}{2}\gamma^2 + \tfrac{1}{6}\gamma^4 - \cdots$$

so the narrow-angle propagator propagates a plane wave at range zero and angle γ into something which approximates a plane wave at range x and angle γ, up to terms in $\gamma^4 x$.

VII. First Example: Scattering from a Knife Edge

In order to demonstrate the superiority of the wide-angle propagator to the narrow-angle propagator, some classical problems with analytical solutions will be considered. The program which will be used is called tropospheric electomagnetic parabolic equation routine (TEMPER), a model which has been developed and improved over the last ten years and was also used in [1] and [2].

The first problem considered is the knife edge. A good reference for this problem is Morse and Feshbach [9, pp. 1383–1387] (see also [14]). The knife edge is the negative z axis, $x = 0, z < 0$, which will be considered a perfect electric conductor. The incident field will be a plane wave e^{ikx} propagating in the positive x direction. The total field scattered from the knife edge is then

$$\frac{1}{\sqrt{i\pi}}[e^{ikr\cos\theta}\Phi(\sqrt{2kr}\sin(\theta/2)) - e^{-ikr\cos\theta}\Phi(-\sqrt{2kr}\cos(\theta/2))] \tag{21}$$

where $-\pi/2 < \theta < 3\pi/2$. This is the solution from [9, p. 1386], modified so the wave travels from left to right, and for Dirichlet boundary conditions. The function

$$\Phi(x) \equiv \int_{-\infty}^{x} e^{is^2}\, ds \tag{22}$$

is related to Fresnel integrals [7, sec. VII-C].

The exact result is shown in Fig. 4 for a plane wave in the x direction. In the third quadrant, one sees mostly the direct plus reflected wave giving a standing wave pattern. In the first and second quadrants, one sees the direct wave plus diffraction from the tip. In the fourth quadrant, one sees diffraction only.

Fig. 5 shows the results from TEMPER using the wide-angle propagator for the same problem. Since the parabolic equation only calculates forward propagation, only the field behind the knife-edge is shown. The source was introduced at the knife-edge as essentially a heaviside function—zero for $z \leq 0$ and one for $z > 0$. Because the knife edge has zero width and is semi-infinite in extent, this problem depends only on the variables kx and kz. Thus, the solution shown in Figs. 4 and 5, when expressed in wavelengths $\lambda = 2\pi/k$, is the solution for any frequency.

To see the differences between the true solution and the solutions computed using the wide-angle and narrow-angle propagators, the field magnitude is plotted in the diffraction region behind the knife edge at 300 wavelengths range increments, as given by the three methods in Fig. 6(a)–(c), respectively. The fields are offset by 3 dB for each range increment for clarity. The wide-angle propagator gives a better approximation to the exact solution than the narrow-angle propagator in the diffraction region. The narrow-angle curves differ from the exact results by 1 dB at about 12.4°. The wide-angle curves differ from the exact results by 1 dB at about

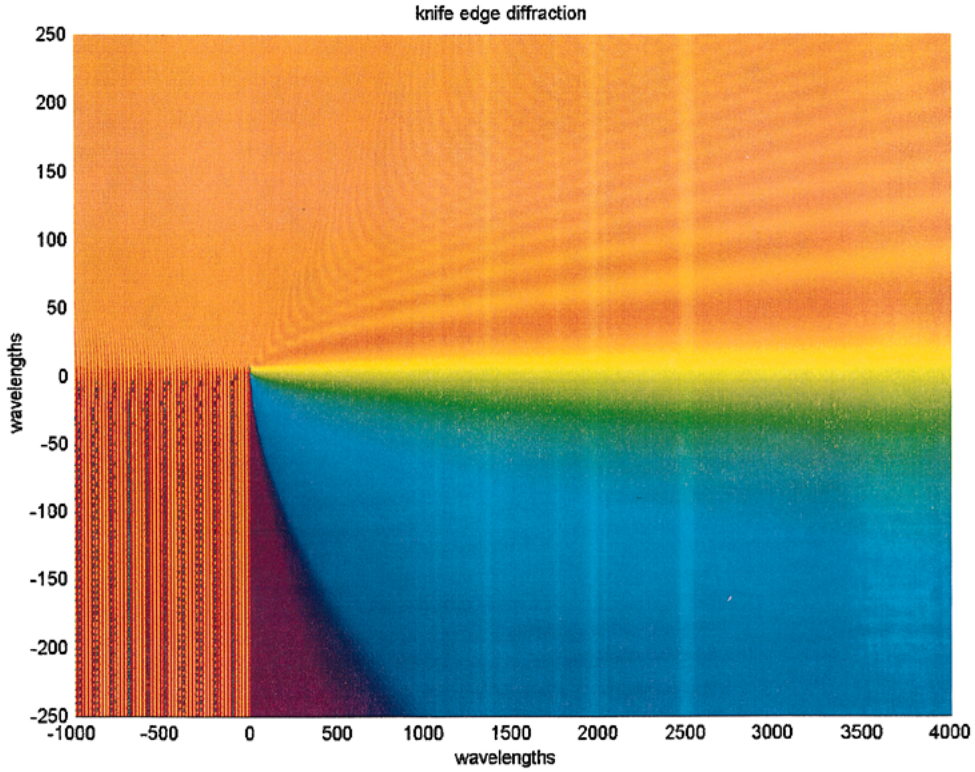

Fig. 4. Reflection and diffraction of plane wave from left by a perfectly conducting knife edge.

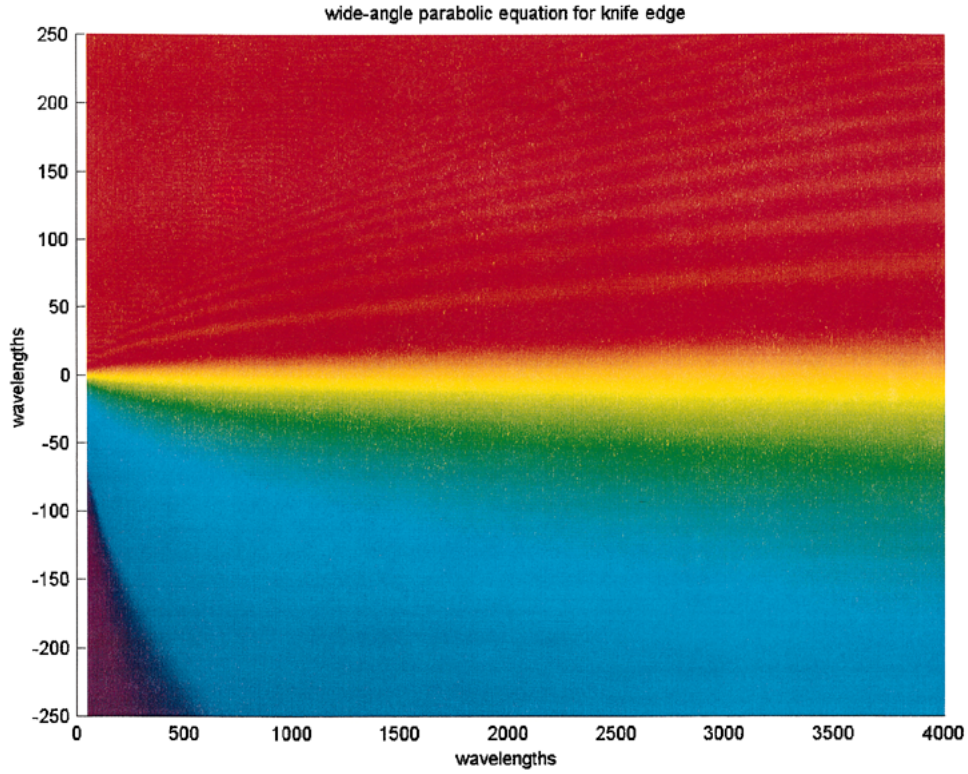

Fig. 5. Propagation behind the knife edge computed by the wide-angle parabolic equation.

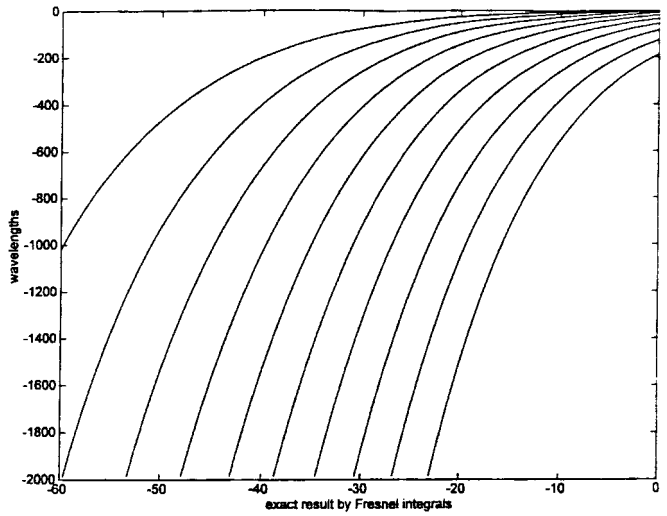

(a)

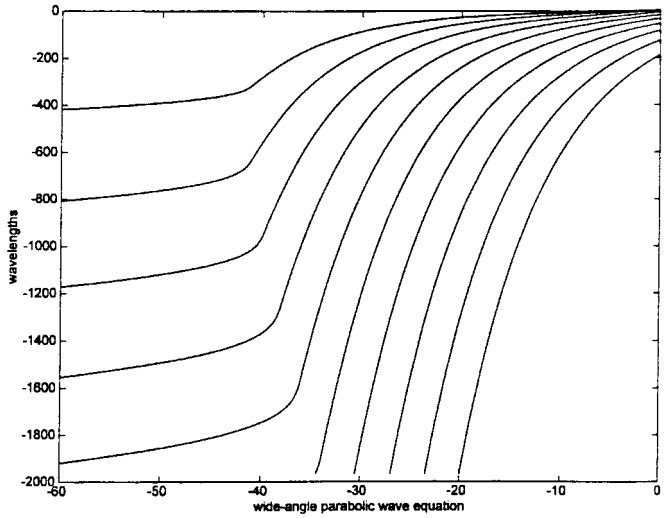

(b)

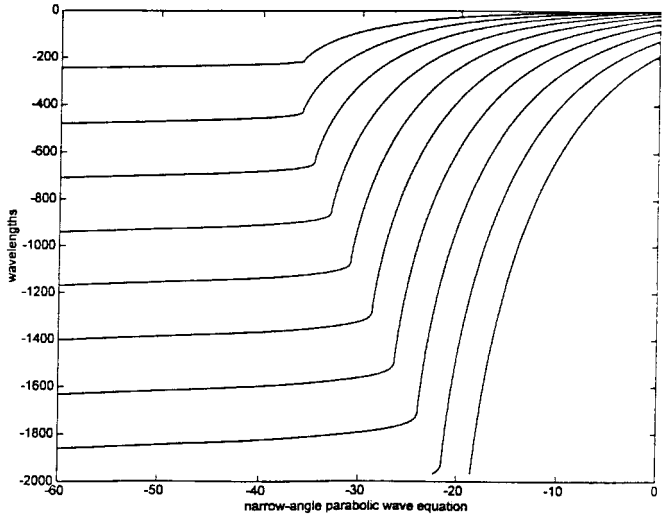

(c)

Fig. 6. Field magnitudes at 300 wavelengths increments behind knife edge. (a) Exact. (b) Wide-angle. (c) Narrow-angle (3-dB offsets for clarity).

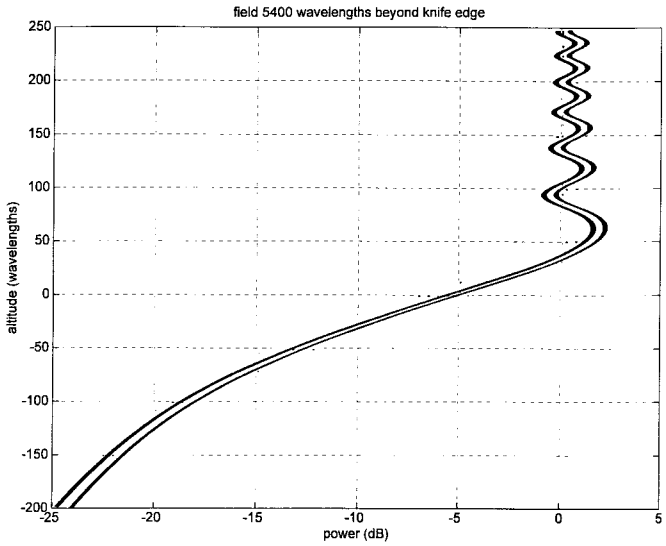

Fig. 7. The field 5400 wavelengths behind the knife edge computed from Fresnel integrals (exact) and by the wide-angle propagator (offset 0.3 dB). They are identical.

13.6°. Fig. 7 shows the exact result from Fresnel integrals and the wide-angle TEMPER calculated field at 5400 wavelengths (offset 0.3 dB) behind the knife edge. Although they are computed by entirely different methods, the fields are identical.

There is no boundary in this problem other than the knife edge. To eliminate artificial boundaries due to the numerical requirement of computing with finite data, the "sin + cos trick" is used. The source is split in two—one half propagated using sine and inverse sine transforms and the other half propagated using cosine and inverse cosine transforms. The sine part propagates as if the source were oddly reflected about the bottom "boundary," while the cosine part propagates as if the source were evenly reflected. Their sum gives the effect of the source propagating without a boundary present, which is what is wanted.

VIII. Second Example: Scattering from a Sinusoidal Surface

In [15], the classical problem of an incident plane wave scattering from a sinusoidal surface was considered. The scattered field is then a sum of plane waves propagating at angles which are related to the angle of incidence by the Bragg law. In [15], the incident field was simulated by using a point source placed far away from the surface. By using a plane wave as the initial field in the parabolic equation, this problem can be redone with better results and used to compare the wide-angle and narrow-angle propagators.

Here is a brief review of how this problem is solved by the parabolic equation. The conformal map [15] $w = f(\xi)$ takes the upper half-plane in $\xi = x + iy$ space onto the region R above the sinusoidal surface in $w = u + iv$ space. If $\Phi(u, v)$ satisfies the Helmholtz equation

$$\frac{\partial^2 \Phi}{\partial u^2} + \frac{\partial^2 \Phi}{\partial v^2} + k^2 \Phi = 0 \quad \text{in } R \tag{23}$$

then the function defined by

$$\phi(x, z) = \Phi(u, v)$$

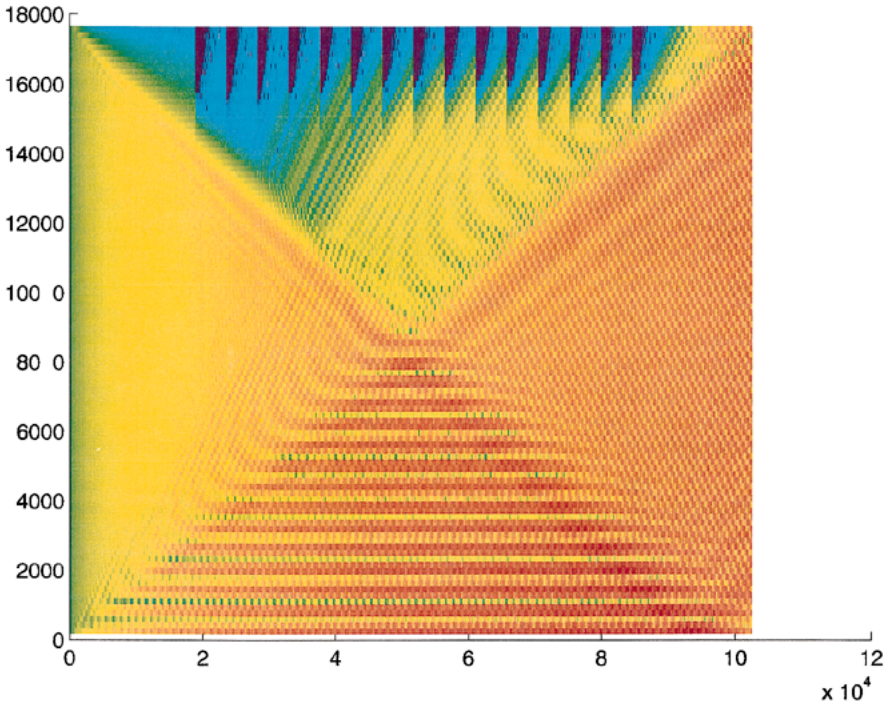

Fig. 8. Scattering of a plane wave of wavelength 34.5 ft and 9.81° incident angle by a sinusoidal surface of amplitude 13 ft and period 1128 ft.

for $x+iy$ and $u+iv$ related by the conformal map satisfies

$$\frac{\partial^2\phi}{\partial x^2}+\frac{\partial^2\phi}{\partial z^2}+k^2|w'|^2\phi=0 \tag{24}$$

in the upper half-plane $z>0$. Thus, free-space propagation over a sinusoidal surface is equivalent to propagation over a flat surface with an index of refraction given by $|w'|$.

Just as in Section II, (24) is factored and only one factor is solved

$$\frac{\partial\phi}{\partial x}=i\sqrt{k^2|w'|^2+\frac{\partial^2}{\partial z^2}}\ \phi. \tag{25}$$

The formal solution is

$$\phi(x,z)=\exp\left[i\int_0^x\sqrt{k^2|w'|^2+\frac{\partial^2}{\partial z^2}}\,dx\right]\phi(0,z). \tag{26}$$

Note the integration is needed because $|w'|$ depends on x. Since $|w'|$ also depends on z, (26) is not an exact solution of (25), because the exponential operator and its x derivative do not commute exactly.

The approximation [5], [6]

$$\sqrt{k^2|w'|^2+\frac{\partial^2}{\partial z^2}}\approx\sqrt{k^2+\frac{\partial^2}{\partial z^2}}+k(|w'|-1). \tag{27}$$

is made. The nearer $|w'|$ is to one, the better the approximation. This is used in (26) and written as

$$\begin{aligned}\phi(x,z)=\exp&\left[\frac{ik}{2}\int_0^x(|w'|-1)\,dx\right]\\ &\exp\left[ix\sqrt{k^2+\frac{\partial^2}{\partial z^2}}\right]\cdot\\ &\exp\left[\frac{ik}{2}\int_0^x(|w'|-1)\,dx\right]\phi(0,z).\end{aligned} \tag{28}$$

This arrangement minimizes the error and is known as the split step. Notice that the middle of the three exponential operators is just the free-space propagator, which is performed as usual by Fourier transforms leading to either the wide-angle or narrow-angle propagators.

For the sinusoidal surface

$$|w'|=1+\frac{2\pi h}{\Lambda}\cos\left(\frac{2\pi x}{\Lambda}\right)\exp\left(-\frac{2\pi z}{\Lambda}\right)$$

where h is the amplitude and Λ is the period of the sinusoid [15]. In this case, the x integration can be done exactly.

The example of [15] is repeated for which the incident angle $\theta_0=9.81°$, $\Lambda=1128$ ft, and $k=2\pi/34.5$. Note that $\theta_{-1},\theta_{-2},\cdots$ are all pure imaginary for this example, giving evanescent waves. In Fig. 8, the field magnitude computed using wide-angle TEMPER is shown. For this problem, a transform size of $T=2^{10}$ was used: $T_0=[T\sin\theta_0]+1$, $\Delta p=(k\sin\theta_0)/T_0$, $\Delta z=\pi/T\Delta p$ and $z_{\max}=T\Delta z$. These choices make the incident plane wave exactly

$$\exp\left(\frac{2\pi iT_0j}{T}\right),\qquad j=0,\cdots,T.$$

A step size of $\Delta r=66$ ft was used and the problem ran for 1548 steps. The finite transform size essentially windows the plane wave and this number of steps is approximately the range

$$\frac{z_{\max}}{\tan\theta_0}$$

where the incident wave is no longer part of the field, and the reflected waves exactly fill the interval $0\le z\le z_{\max}$. A filter was applied in z-space every 100 range steps, but it was not applied before step 400 or after step 1300, so the full incident field could propagate and the full reflected field

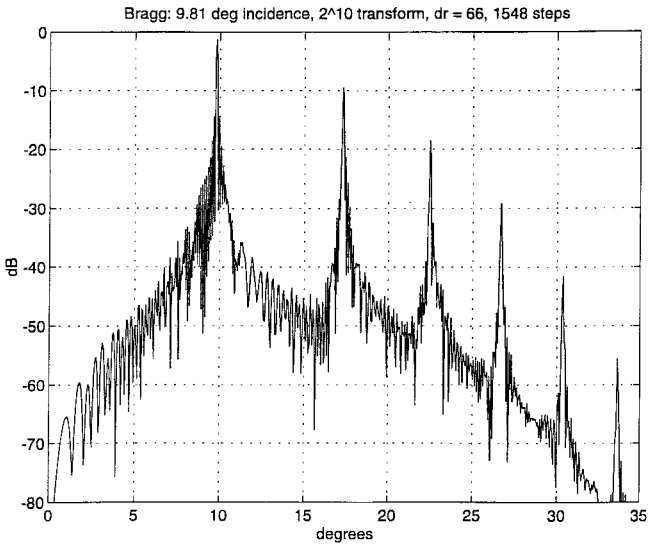

Fig. 9. Magnitude of the transform of the field scattered by the sinusoidal surface at the final range.

TABLE I
EXACT BRAGG ANGLES (DEGREES) AND AMPLITUDES (DECIBELS) FOR 9.81° INCIDENT PLANE WAVE WITH $k = 2\pi/34.5, h = 13$ ft, $\Lambda = 1128$ ft, COMPARED WITH THE WIDE-ANGLE AND NARROW-ANGLE PROPAGATOR SOLUTIONS, $T = 2^{10}, \Delta r = 66$ ft, AND 1548 STEPS

exact Bragg		wide-angle		narrow-angle	
angles	amplitudes	angles	amplitudes	angles	amplitudes
9.81	- 1.23	9.81	- 1.30	9.81	- 1.21
17.29	- 9.20	17.27	- 9.57	17.51	-10.01
22.45	-18.22	22.44	-18.55	22.92	-18.99
26.67	-28.75	26.67	-29.18	27.48	-30.75
30.34	-40.56	30.35	-41.63	31.52	-43.87
33.65	-53.45	33.64	-55.51	35.33	-58.64

could reach the final range. The action of the filter can be seen as the blue "notches" at top of Fig. 8. The angles and amplitudes of the reflected plane waves were found by taking the discrete sine transform of the field there and normalizing it by $2/T$. The magnitude of the result from the wide-angle TEMPER calculation is shown in Fig. 9. The numerical values of the computed angles and amplitudes are shown in Table I along with the exact amplitudes and amplitudes from (A.4) and (A.9) and the corresponding results for the narrow-angle propagator. As expected, there is excellent agreement using the wide-angle propagator, and somewhat lesser performance with the narrow-angle propagator.

The complete total field $E^{\text{inc}} - E^{sc}$ in Fig. 8 is the triangular portion showing a sequence of horizontal bands. This is because the total field is just a perturbation of $E^{\text{inc}} - E_0$, the direct and specular, which is

$$\exp[ikx\cos\theta_0](\exp[-ikz\sin\theta_0] - \exp[ikz\sin\theta_0])$$

and has magnitude

$$2\sin(kz\sin\theta_0)$$

independent of x and periodic in z. This may be contrasted with [3, fig. 4], showing "the onset of Bragg scattering," where the bands fan out in a radial pattern due to the use of a distant point source as the incident field.

APPENDIX
BRAGG SCATTERING

The exact solution for scattering from a perfectly conducting sinusoidal surface is reviewed. Let the surface be given by $z = h\sin(2\pi x/\Lambda)$ and let the incident field be a plane wave at angle θ_0

$$E^{\text{inc}} = \exp[ik(x\cos\theta_0 - z\sin\theta_0)]. \tag{A.1}$$

Write the scattered field E^{sc} as a series in powers of kh, the electrical amplitude of the sinusoid,

$$E^{sc} = \sum_{m=0}^{\infty} (hk)^m E_m. \tag{A.2}$$

Each of the terms E_m is a sum of $2m+1$ plane waves

$$E_m = \sum_{j=-m}^{m} B(m,j)\exp[ik(x\cos\theta_j + z\sin\theta_j)] \tag{A.3}$$

where the angles θ_j turn out to be related to θ_0 by the Bragg law

$$k\cos\theta_j = k\cos\theta_0 - j\frac{2\pi}{\Lambda}. \tag{A.4}$$

Since the surface is a perfect electric conductor, the total field vanishes on the surface. Thus, write the total field as $E^{\text{inc}} - E^{sc}$ so that $E^{\text{inc}} = E^{sc}$ on the surface and

$$\exp\left[ik\left(x\cos\theta_0 - h\sin\theta_0\sin\left(\frac{2\pi x}{\Lambda}\right)\right)\right] = \sum_{m=0}^{\infty}(kh)^m \sum_{j=-m}^{m} B(m,j)\exp \cdot\left[ik\left(x\cos\theta_j + h\sin\theta_j\sin\left(\frac{2\pi x}{\Lambda}\right)\right)\right]. \tag{A.5}$$

Divide by the left side of (A.5) to get

$$1 = \sum_{m=0}^{\infty}(kh)^m \sum_{j=-m}^{m} B(m,j)\xi^j e^{khK_j\xi^{-1}} e^{-khK_j\xi} \tag{A.6}$$

where

$$\xi = e^{-2\pi x/\Lambda}, \quad K_j = \tfrac{1}{2}(\sin\theta_j + \sin\theta_0).$$

Expanding the exponentials into their Taylor series, (A.6) becomes

$$1 = \sum_{m=0}^{\infty}\sum_{j=-m}^{m}\sum_{p=0}^{\infty}\sum_{q=0}^{\infty} \cdot (kh)^{m+p+q}\xi^{j-p+q}B(m,j)K_j^{p+q}\frac{(-1)^q}{p!q!}. \tag{A.7}$$

Now set $M = m+p+q, N = j-p+q$. Since $-m \le j \le m$, this implies $2p \le M-N, 2q \le M+N$ and since $p \ge 0, q \ge 0$, it follows that $-M \le N \le M$.

Thus, equating the coefficients of each power of kh and each power of ξ in (A.7), for each $M = 0, 1, 2, \cdots$ and each N satisfying $-M \le N \le M$

$$\delta(M) = \sum_{p=0}^{[(M-N)/2]} \sum_{q=0}^{[(M+N)/2]} B(M-p-q, N+p-q) \cdot K_{N+p-q}^{p+q} \frac{(-1)^q}{p!q!}. \tag{A.8}$$

In particular, $B(0,0) = 1$, i.e., the zero-order term is just specular reflection and for $M = 1, 2, \cdots$, and N satisfying $-M \le N \le M$

$$\begin{aligned} B(M,N) = &- \sum_{p=1}^{[(M-N)/2]} B(M-p, N+p) K_{N+p}^{p} \frac{1}{p!} \\ &- \sum_{q=1}^{[(M+N)/2]} B(M-q, N-q) K_{N-q}^{q} \frac{(-1)^q}{q!} \\ &- \sum_{p=1}^{[(M-N)/2]} \sum_{q=1}^{[(M+N)/2]} B(M-p-q, N+p-q) \\ &\cdot K_{N+p-q}^{p+q} \frac{(-1)^q}{p!q!} \end{aligned} \tag{A.9}$$

which gives a recursive formula for the $B(M,N)$. The coefficient of the plane wave scattered at angle θ_N is then

$$\sum_{m=N}^{\infty} (kh)^m B(m,N). \tag{A.10}$$

ACKNOWLEDGMENT

The author would like to thank L. Fishman and M. Levy for pointing out the exact expression for the wide-angle propagator and for suggesting [9] and [10].

REFERENCES

[1] J. R. Kuttler and G. D. Dockery, "Theoretical description of the parabolic approximation/Fourier split-step method of representing electromagnetic propagation in the troposphere," *Radio Sci.*, vol. 26, pp. 381–393, 1991.
[2] G. D. Dockery and J. R. Kuttler, "An improved impedance boundary algorithm for Fourier split-step solutions of the parabolic wave equation," *IEEE Trans. Antennas Propagat.*, vol. 44, pp. 1592–1599, Dec. 1996.
[3] D. J. Donohue and J. R. Kuttler, "Modeling radar propagation over terrain," *Johns Hopkins APL Tech. Dig.*, vol. 18, pp. 279–287, 1997.
[4] ——, "Propagation modeling over terrain using the parabolic wave equation," *IEEE Trans. Antennas Propagat.*, to be published.
[5] M. D. Feit and J. A. Fleck, "Light propagation in graded-index optical fibers," *Appl. Opt.*, vol. 17, pp. 3990–3998, 1978.
[6] D. J. Thomson and N. R. Chapman, "A wide-angle split-step algorithm for the parabolic equation," *J. Acoust. Soc. Amer.*, vol. 74, pp. 1848–1854, 1983.
[7] M. Abramowitz and I. A. Stegun, *Handbook of Mathematical Functions*. Washington, DC: Nat. Bureau Standards, 1964.
[8] H. S. Carslaw and J. C. Jaeger, *Conduction of Heat in Solids*, 2nd ed. New York: Oxford, 1959.
[9] P. M. Morse and H. Feshbach, *Methods of Theoretical Physics*. New York: McGraw-Hill, 1953.
[10] N. W. McLachlan, *Bessel Functions for Engineers*, 2nd ed. New York: Oxford, 1955.
[11] H. Bateman, *Tables of Integral Tranforms*. New York: McGraw-Hill, 1954, vol. I.
[12] C. A. Balanis, *Antenna Theory*. New York: Harper Row, 1982.
[13] D. E. Kerr, *Propagation of Short Radio Waves*. New York: McGraw-Hill, 1951.
[14] M. Born and E. Wolf, *Principles of Optics*, 2nd ed. New York: Macmillan, 1964.
[15] J. R. Kuttler and J. D. Huffaker, "Solving the parabolic wave equation with a rough surface boundary condition," *J. Acoust. Soc. Amer.*, vol. 94 , pp. 2451–2454, 1993.

James R. Kuttler, for a photograph and biography, see p. 1599 of the December 1996 issue of this TRANSACTIONS.